Optogenetic mapping of local inhibitory circuitry in cerebellum reveals spatially biased coordination of interneurons via electrical synapses

Jinsook Kim, Soojung Lee, Sachiko Tsuda, Xuying Zhang, Brent Asrican, Bernd Gloss, Guoping Feng, and George J. Augustine

Supplemental Information

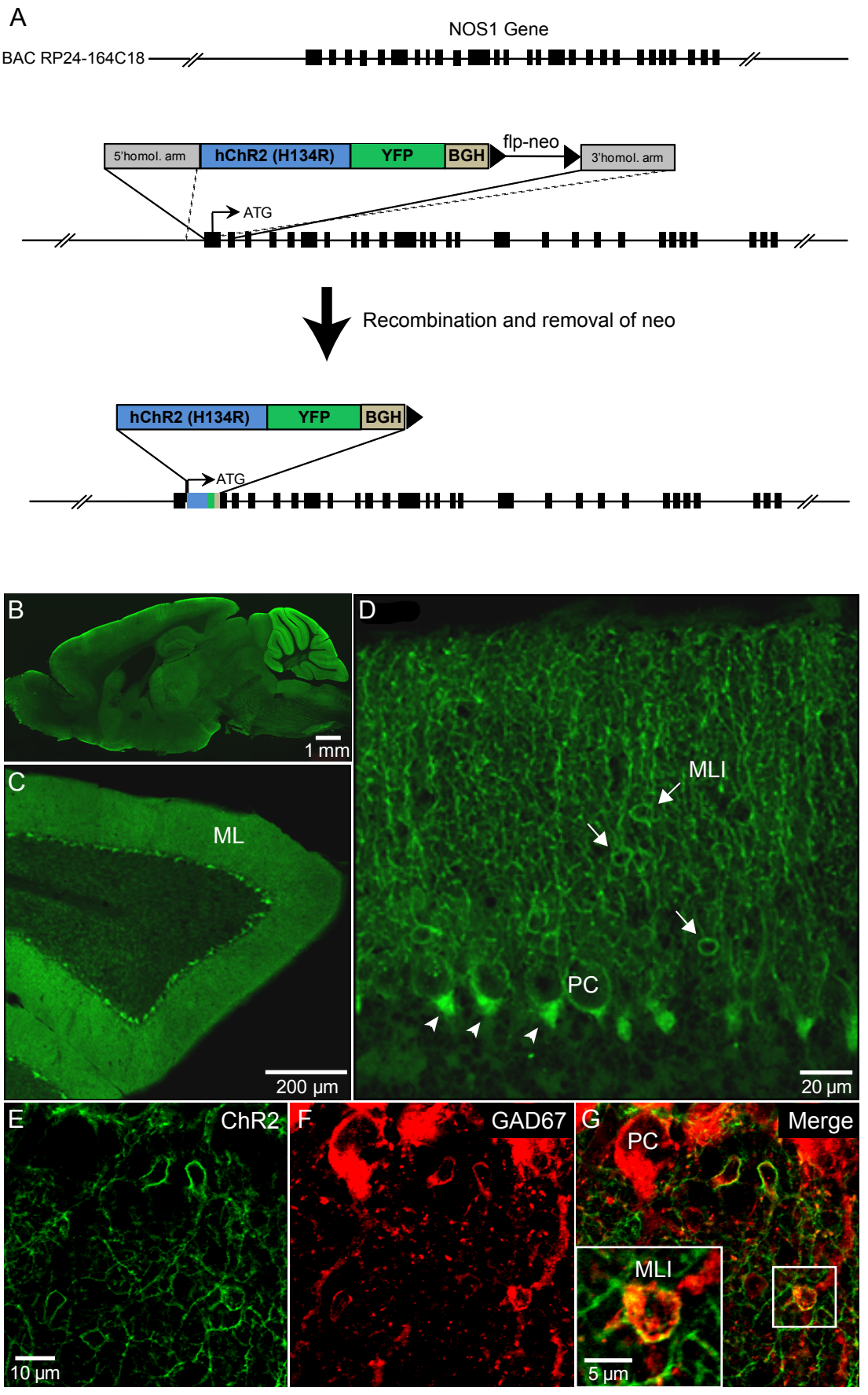

Figure S1. Selective expression of ChR2-YFP in cerebellar molecular layer interneurons

(A) Schematic of BAC recombination scheme used to generate the nNOS-hChR2(H134R)-YFP BAC transgene. The mouse BAC containing a neuronal form of nitric oxide synthase 1 (nNOS1) was obtained from CHORI (RP24-164C18) and modified as outlined in this figure. The BAC insert has a total length of 173341bp and is derived from chromosome 5. The cDNA for a fusion protein of hChR2 (H134R) and YFP was inserted into exon 1 by recombineering in bacteria. The modified BAC was linearized with Nru I, gel purified, electroeluted and dialyzed. hChR2, humanized ChR2 cDNA mutated at amino acid position 134 His to Arg (H134R); YFP, yellow fluorescent protein; BGH, bovine growth hormone polyadenylation signal; flp-neo, FRT sites flanked neomycin resistance gene.

(B) Image of YFP fluorescence (green) in a sagittal section from an adult transgenic mouse brain. Fluorescence is observed throughout the brain, but is highest in the cerebellum.

(C) Higher-magnification image reveals that the molecular layer (ML) of the cerebellar cortex has the highest level of transgene expression.

(D) Most interneurons in the molecular layer express ChR2-YFP in the plasma membrane of their somata (arrows) and dendrites. Strong YFP fluorescence associated with basket cell axons is observed in pericellular baskets around PC soma and pinceau terminals (arrowheads) surrounding the PC axon hillock.

(E – G) Double labeling of ChR2-expressing cerebellar slices. (E) YFP fluorescence in cerebellar MLI. (F) Image of GAD67 immunostaining of the area shown in E. (G) Merger of the images shown in E (green) and F (red) reveal that while both MLI and PCs are positive for GAD67, only MLI express ChR2-YFP. Area in white square is enlarged in the inset, to illustrate MLI expressing both proteins.

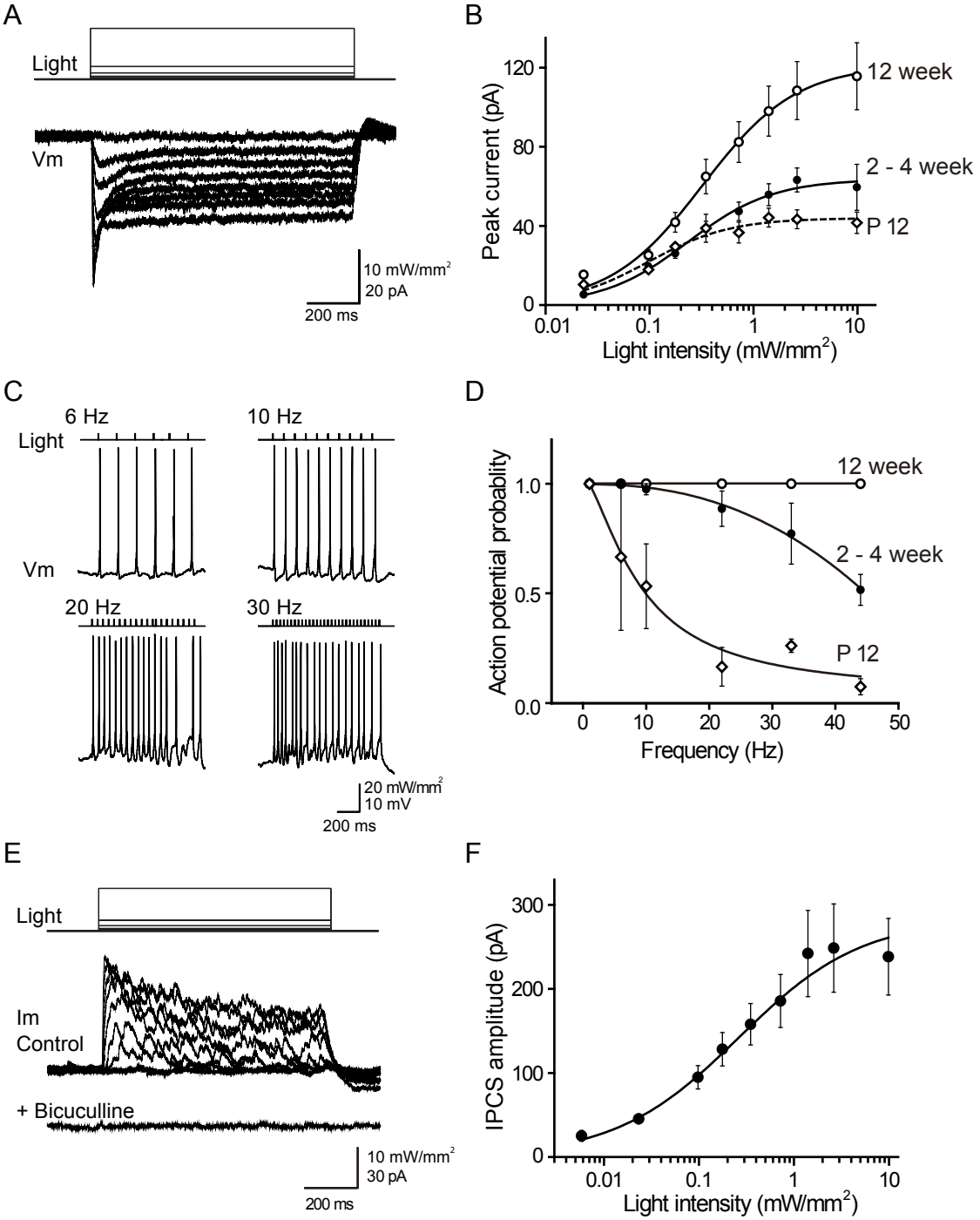

Figure S2. Light-induced control of MLI and their inhibitory circuit with Purkinje cells

(A) Photocurrents (Im) induced by illumination (Light) of a voltage-clamped MLI expressing ChR2. The amplitude of these photocurrents depended upon light intensity. Holding potential was -70 mV.

(B) Relationship between light intensity and peak amplitude of photocurrent evoked in MLI from mice of different ages (n = 8). Photocurrent amplitude increased both with light intensity and mouse age.

(C) Varying the frequency of light flashes (5 ms, 9.9 mW/mm^2) caused proportional changes in action potential frequency in a ChR2-expressing interneuron.

(D) Relationship between frequency of photostimulation and action potential probability in MLI at different ages (P12, n = 8; 2-4 weeks, n = 18; 12 weeks, n = 8). Probability of evoking action potentials decreased as a function of light pulse frequency, with a higher roll-off frequency observed in older mice.

(E) IPSCs (Im) evoked in a Purkinje cell in response to photostimulation (Light) of ChR2-expressing MLI. IPSC amplitude increased with increasing light intensity. Holding voltage was - 55 mV and the internal solution contained low Cl, resulting in outward IPSCs. These IPSCs were completely blocked by $GABA_A$ receptor antagonist, bicuculline (10 μM).

(F) Relationship between light intensity and IPSC amplitude in Purkinje cells (n = 9).

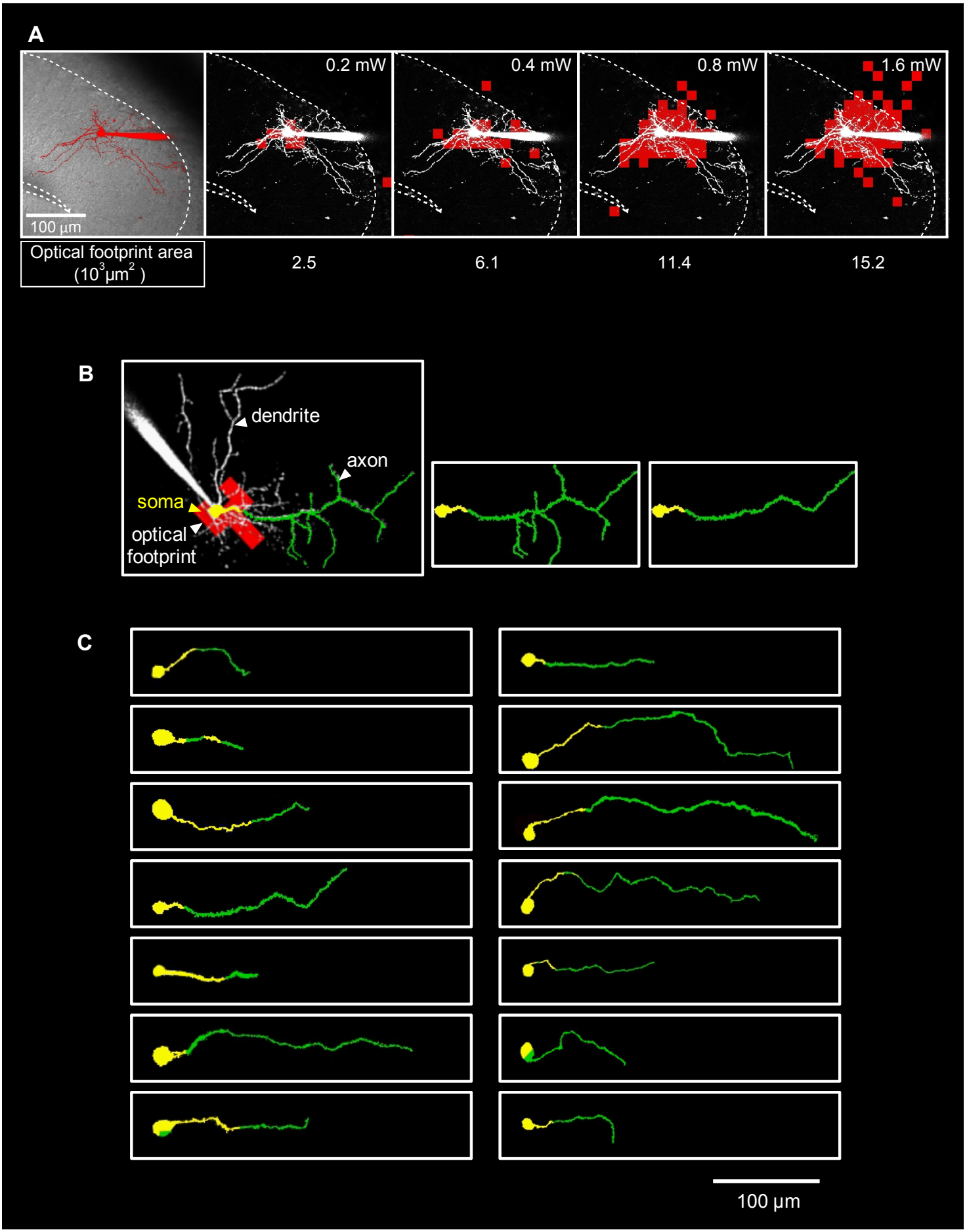

Figure S3. Spatial resolution of MLI photostimulation

(A) Relationship between photostimulus intensity and optical footprint size. Left panel: Image of a patch clamped basket cell filled with Alexa 594 dye (red). Other panels: Scanning a laser light spot across the brain slice, while simultaneously measuring membrane potential changes in the ChR2-expressing basket cell, revealed locations where photostimulation evoked action potentials in the basket cell. Red indicates the locations where action potentials were induced (optical footprint), while white indicates the structure of the cell (same image as in left panel, except fluorescence is now indicated by white). As laser spot intensity increased (labels in upper right corners), the optical footprint area (numbers at bottom) became larger.
(B-C) The extent of overlap between axon and optical footprint. (B) (Left) Example of an MLI optical footprint (area where light spots evoked action potentials in MLI; red) superimposed on a fluorescence image of the MLI. Axonal structures that do not overlap]with the optical footprint are colored green while parts of the cell (soma and proximal axons) that overlaps with the optical footprins are yellow. (Middle) Image of the entire MLI, showing areas where action potential were evoked (yellow) and not evoked (green). (Right) Image of cell soma and primary axon to emphasize the extent of overlap between axon and optical footprint. (C) Smilar images of soma and main axon for many MLI. Area of overlap between optical footprint and cell is yellow and non-overlapping (axonal) area is green. In every case, overlap between axon and optical footrpint occurred only near the cell soma.

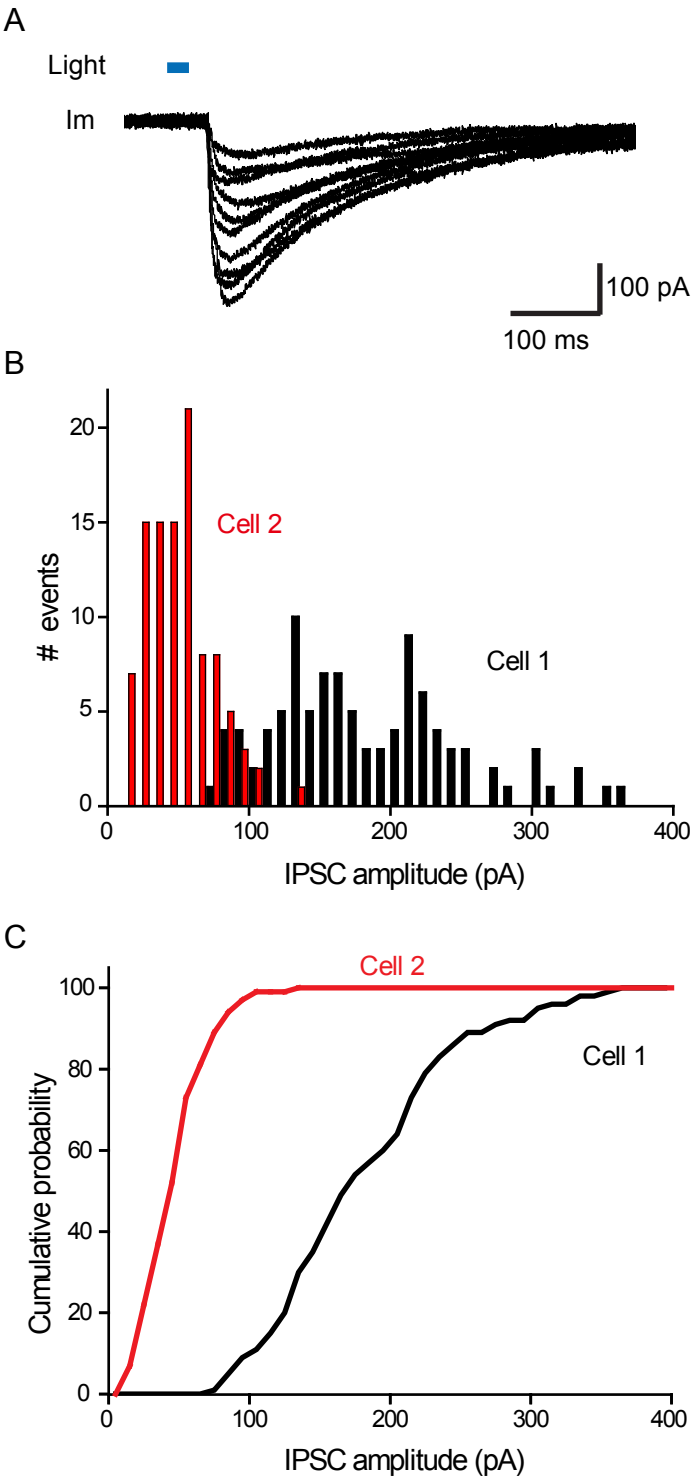

Figure S4. Fluctuations in amplitude of light-evoked IPSCs

(A) IPSCs (Im) evoked in a Purkinje cell in response to a series of minimal photostimuli (Light, 5 ms duration) applied to a fixed location. IPSC amplitudes fluctuate markedly among trials.

(B) Distribution of IPSC amplitudes measured in two different Purkinje cells. Traces in (A) were recorded in Purkinje cell 1.

(C) Cumulative probability distributions for IPSCs recorded in the two Purkinje cells shown in (B).

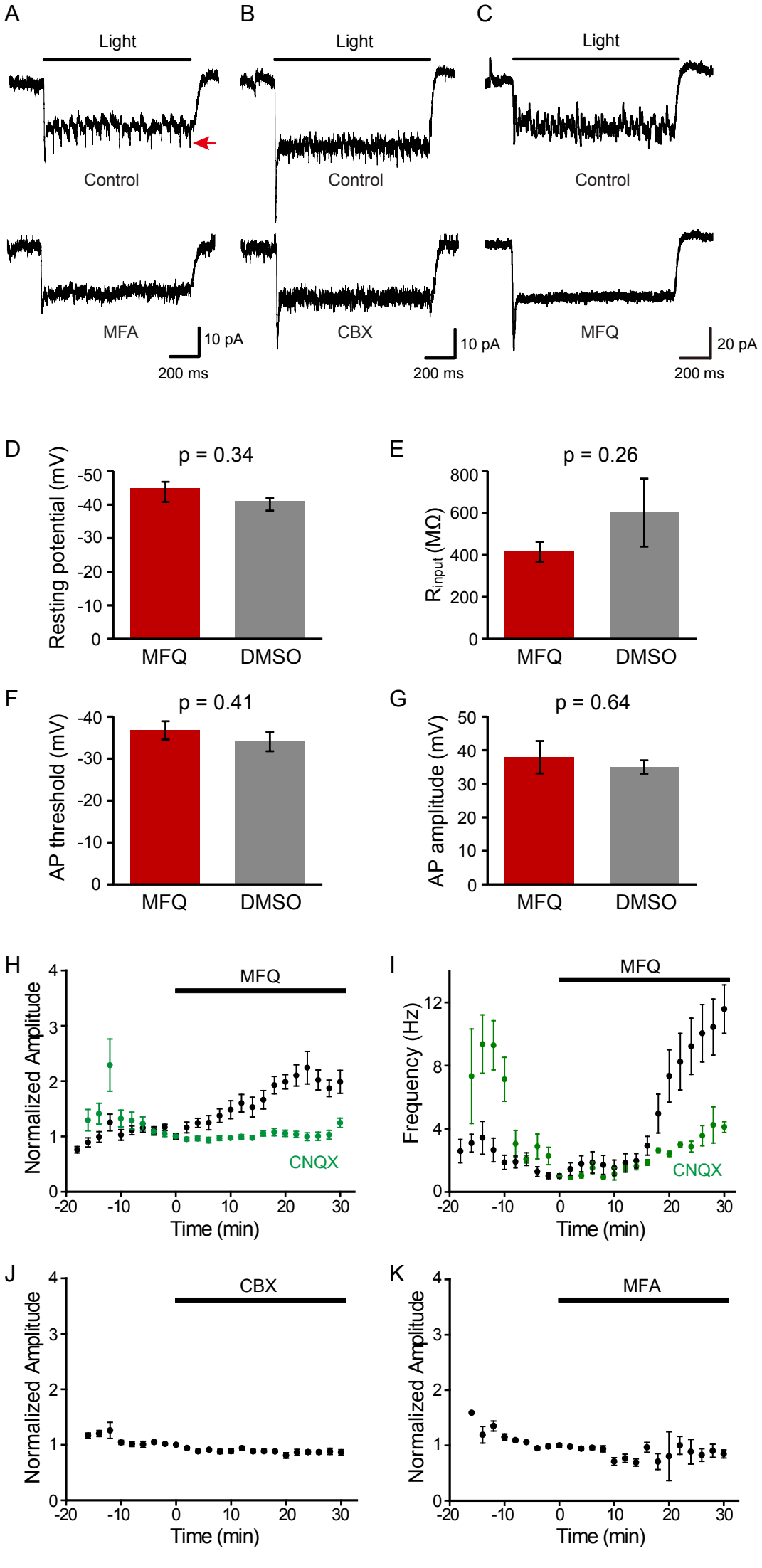
A
B
C
Light
Light
Light
Control
Control
Control
MFA
CBX
MFQ
10 pA
200 ms
10 pA
200 ms
20 pA
200 ms
D
p = 0.34
Resting potential (mV)
-50
-40
-30
-20
-10
0
MFQ
DMSO
E
p = 0.26
R_{input} (MΩ)
800
600
400
200
0
MFQ
DMSO
F
p = 0.41
AP threshold (mV)
-40
-30
-20
-10
0
MFQ
DMSO
G
p = 0.64
AP amplitude (mV)
50
40
30
20
10
0
MFQ
DMSO
H
MFQ
Normalized Amplitude
4
3
2
1
0
CNQX
-20
-10
0
10
20
30
Time (min)
I
MFQ
Frequency (Hz)
12
8
4
0
CNQX
-20
-10
0
10
20
30
Time (min)
J
CBX
Normalized Amplitude
4
3
2
1
0
-20
-10
0
10
20
30
Time (min)
K
MFA
Normalized Amplitude
4
3
2
1
0
-20
-10
0
10
20
30
Time (min)

Figure S5. Analysis of pharmacological agents used to study electrical coupling between MLI

(A-C) Electrical coupling between interneurons observed by photostimulation. Upper: Recordings from MLI revealed that illuminating the slice caused an inward photocurrent in the neuron, as well as spikelets (arrow). Recordings made while chemical synapses were blocked by treatment with APV (50 μM), CNQX (10 μM) and PTX (100 μM). Spikelets were inhibited by treatment with 3 different gap junction blockers (lower panels): (A) MFA (200 μM), (B) CBX (200 μM), (C) MFQ (50 μM). Interneurons were held at a potential -60 or -70 mV.

(D-G) Comparison of resting membrane potential (D), input resistance (E), action potential threshold (F) and action potential amplitude (G) measured during MFQ treatment (red, n = 6) or treatment with DMSO vehicle (0.05%; grey, n = 5). MFQ treatment did not cause any significant change in the electrical properties of MLI.

(H-I) Effects of MFQ on amplitude (H) and frequency (I) of miniature postsynaptic currents (mPSCs) recorded in Purkinje cells treated with TTX (1 μM).

(H) mPSC amplitude was increased by 50 μM MFQ (black). This increase was absent when slices were treated with CNQX (10 μM; green), indicating that MFQ mainly increased the amplitude of miniature EPSCs (n = 3).

(I) mPSCs frequency was dramatically increased by 50 μM MFQ (black).This increase was largely prevented by treatment with CNQX (10 μM; green), indicating that MFQ mainly increased the frequency of miniature EPSCs (n = 3).

(J-K) Treatment with 200 μM CBX (J, n = 4) and MFA (K, n = 3) caused only subtle reductions in mPSC amplitude.

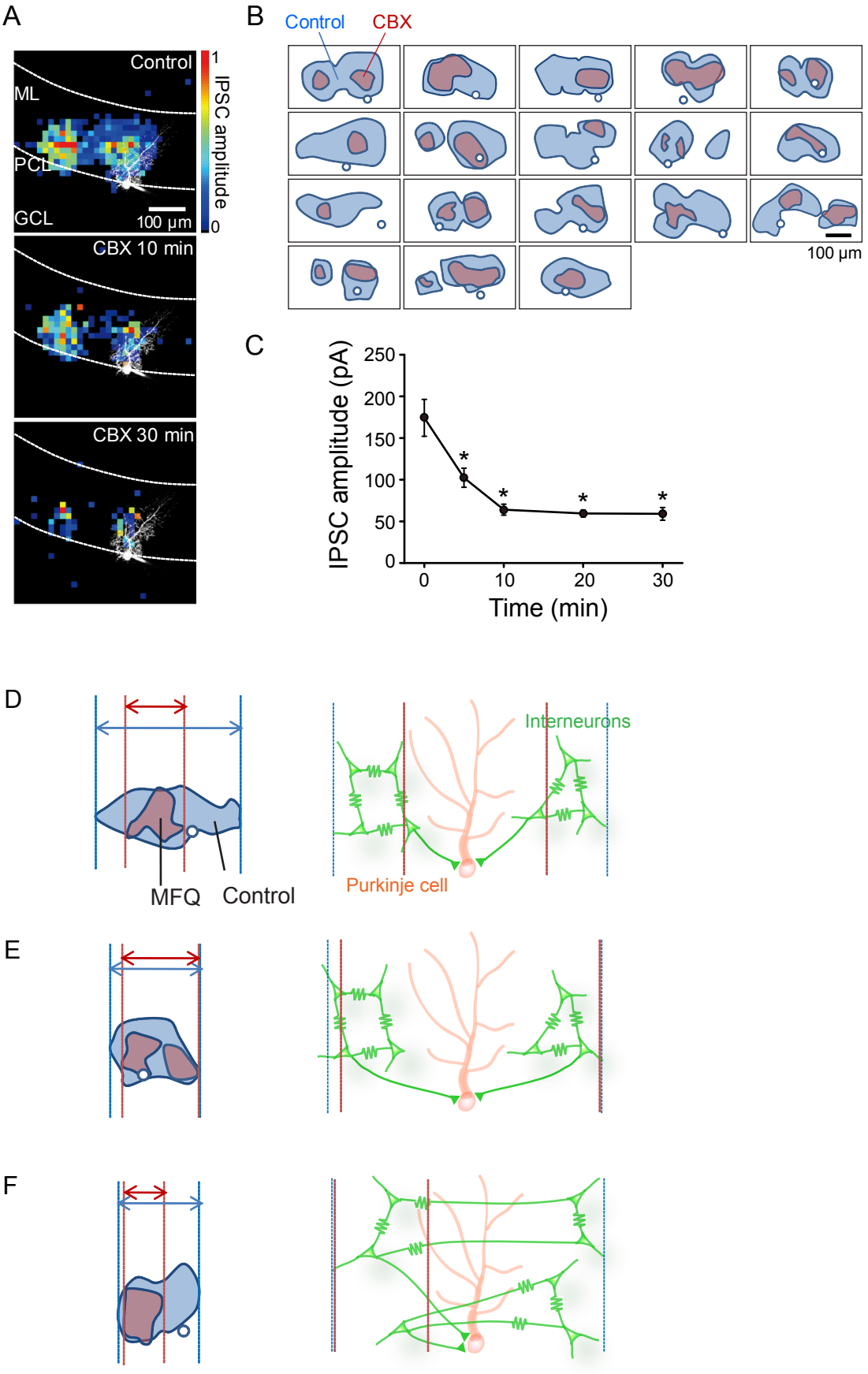

Figure S6. Spatial organization of the inhibitory input field of Purkinje cells

(A-C) CBX reduces inhibitory input field of Purkinje cells

(A) Inhibitory input field size of a Purkinje cell (top panel) was reduced by treatment with CBX (200 μM), as shown in the 2 maps recorded 10 minutes (center) and 30 minutes (bottom) after starting CBX treatment. Pseudocolor scale indicates the normalized amplitude of IPSCs evoked by light at each location. Image of dye-filled Purkinje cell is shown in white.

(B) Gallery of input field maps measured for 18 different Purkinje cells before and after CBX treatment. Outlines of input fields measured in control conditions are shown in blue and those measured in the same experiments after CBX treatment are shown in pink. In every case, CBX treatment reduced the area of the input field. White circles indicate the location of somata of Purkinje cells used for input field measurements.

(C) Time course of reductions in the mean amplitude of IPSCs during CBX treatment. Asterisks indicate time points where CBX treatment caused significant reductions in amplitude ($P<0.001$).

(D-F) Comparison of input field maps before and after treatment with gap junction blockers. Left: Comparison of the width of input fields before (blue) and after (pink) blocking electrical synapses with MFQ. Right: interpretation of organization of circuits underlying input maps shown on the left.

(D) In some cases (10 out of 38 experiments), gap junction blockers (MFQ and CBX) narrowed the width of the input field (left). This indicates that the electrically coupled MLI lie beyond the MLI that directly innervate a Purkinje cell (right).

(E) In other cases (12 out of 38 experiments), gap junction blockers had little effect on the width of the input map. This is expected if the electrically coupled MLI are located between the MLI and Purkinje cells that are connected by chemical synapses.

(F) In the remainder of the cases (16 out of 38 experiments), gap junction blockers selectively reduced the input field on just one side. In these cases, it is likely that the electrically coupled MLI are on the opposite side of the Purkinje cell from the MLI that are directly innervating the Purkinje cell.

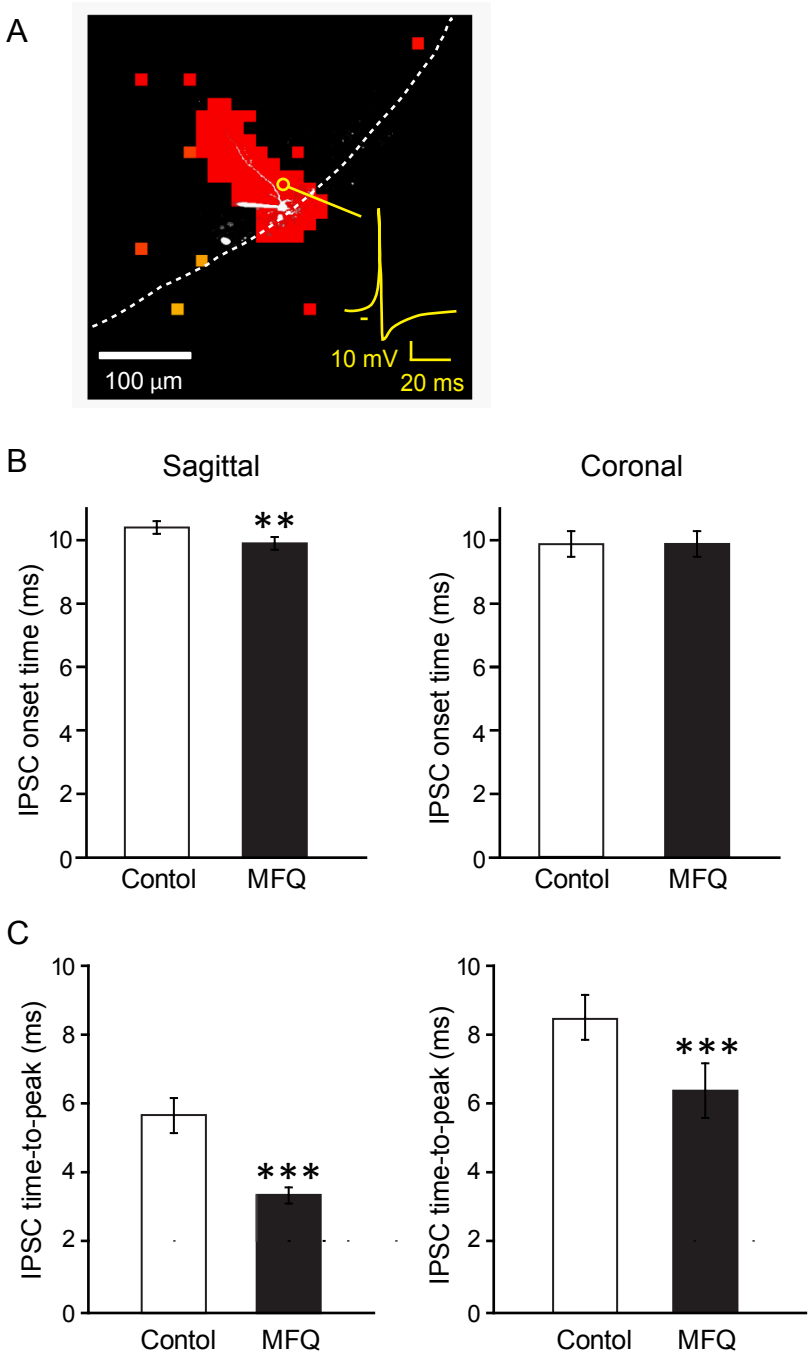

Figure S7. Photostimulation of MLI in coronal cerebellar slices

(A) Optical footprint of interneuron in a coronal cerebellar slice. Area where photostimulation evoked action potentials in MLI in coronal slices was revealed by scanning the light spot across the slice while simultaneously measuring membrane potential changes in a ChR2-expressing MLI (right). Red indicates locations where the light spot evoked action potentials. Yellow trace indicates an action potential evoked by photostimulation at the circled location, while dashed line indicates location of Purkinje cell layer.

(B-C) Effect of MFQ on IPSC kinetics in sagittal and coronal sections.

(B) MFQ treatment caused a decrease (**p<0.01, paired t-test) in the mean latency of IPSCs in sagittal slices (left, n = 20) but not coronal slices (right, n = 14).

(C) MFQ treatment caused a significant decrease in the mean time-to-peak of IPSCs in both sagittal (left, n = 20) and coronal (right, n = 14) slices (***p<0.001, paired t-test).

Supplemental Experimental Procedures

Generation of transgenic mice expressing ChR2

BAC transgenic mice expressing channelrhodopsin-2 (ChR2) under the control of the nNOS promoter were generated by microinjection of a modified BAC into fertilized eggs. BAC clone RP24-164C18 contains 173341bp of C57Bl6 DNA from chromosome 5. This BAC includes the entire nNOS gene (Nitric oxide synthase, brain) with a length of 86973 bp encoding 28 exons and about 37 kb of upstream sequence (see supplementary figure S1). In order to recombine the cDNA encoding a fusion protein of hChR2 (H134R) and YFP into this BAC, we constructed a targeting vector from which we derived a targeting fragment for recombineering. The targeting fragment consisted of a 435bp homology region (A-Box) immediately upstream of the ATG in the nNOS gene. The hChR2 (H134R)-YFP cDNA was fused to the A-Box replacing the nNOS ATG with the hChR2 ATG. At the 3' end of the hChR2 (H134R)-YFP cDNA a synthetic bovine growth hormone (BGH) polyadenylation signal was added after the STOP codon. For selection of recombined BACs, a flipase-site flanked neomycin resistance gene was incorporated into the targeting fragment following the cDNA. Finally the 3' end of the targeting fragment contained a 491bp homology region (B-Box) starting 132bp downstream of the nNOS ATG. Recombineering was according to a protocol developed in the Copeland lab. In brief, the targeting fragment was electroporated into induced EL250 bacteria harboring the nNOS BAC. Recombined colonies were selected on Chloramphenicol/Kanamycin plates and screened by colony PCR. The neo gene was removed from the recombined BAC by arabinose driven flipase expression.

Recombined BACs without the neo marker were linearized by restriction enzyme digestion using Nru I, gel purified and electro-eluted from the gel slice. After filter dialysis with a Millipore VSWP02500 filter, the BAC fragment concentration was adjusted to 1ng/µl and microinjected into pronuclei of B6SJLF1 mouse oocytes. We obtained four independent founder

lines of nNOS-hChR2(H134R)-YFP BAC transgenic mice. Line number 3 is described in this paper.

Genotyping of nNOS-hChR2(H134R)-YFP transgene in founder animals was done using the following primers: BGH-F (forward primer) 5'-CTT CTG AGG CGG AAA GAA CC-3' and dNOS4 (reverse primer) 5'-TCT GCT TTG GCT GGT CCC-3'. PCR protocol is 30 cycles of 94°C 30 sec., 55°C 30 sec., 72°C 30 sec. The PCR product is 660 bp.

Anatomy and immunohistochemistry

To assess the expression of ChR2-YFP, mice (P21, P31, P150) were deeply anesthetized with ketamine/xylazine and perfused transcardially with 4% paraformaldehyde in 0.1M phosphate buffered saline (PBS). Brains were immersed in the same fixative overnight at 4°C, cryoprotected with 30% sucrose in PBS until equilibrated, and cut on a freezing microtome into 40 µm thick sagittal sections. For detecting GAD67 expression, brain sections were blocked with 10% normal goat serum in PBS for 1 hr, followed by the incubation with monoclonal mouse anti-GAD67 (1:1000, Chemicon) at 4°C for 48 hr. Sections were then incubated with secondary Alexa 555-conjugated goat anti-mouse antibody (1:200, Invitrogen) for 2 hr. Sections were imaged with a widefield fluorescence microscope (Nikon Eclipse Ti Inverted Microscope System) or a laser-scanning confocal microscope (Zeiss LSM510 META).

Brain slice recording

Transgenic mice were killed by decapitation under deep halothane anesthesia and the cerebellum was quickly removed. All procedures were conducted according to the Institutional Animal Care and Use Committee guidelines of the Biopolis Biological Resource Center (BRC), Duke University, and the Marine Biological Laboratory. 250 or 300 µm thick cerebellar slices from mice ranging from 12 days to 12 weeks of age were used to measure ChR2-induced activation of interneurons, while 300 µm thick sections from mice aged between 21 days to 34

days were used for mapping studies. Cerebellar sections were cut in ice-cold cutting solution using a vibratome as previously described (Lee et al., 2010). The cutting solution contained (in mM) 250 sucrose, 26 $NaHCO_3$, 10 glucose, 4 $MgCl_2$, 3 myo-inositol, 2.5 KCl, 2 sodium pyruvate, 1.25 $NaHPO_4$, 0.5 ascorbic acid, 0.1 $CaCl_2$, 1 kynurenic acid and was bubbled with 95% O_2/5% CO_2. After cutting, slices were kept for at least 1 hr in the standard extracellular solution which contained (in mM): 126 NaCl, 24 $NaHCO_3$, 1 NaH_2PO_4, 2.5 KCl, 2.5 $CaCl_2$, 2 $MgCl_2$, 10 glucose, 0.4 ascorbic acid (pH 7.4 when equilibrated with 95% O_2/5% CO_2). Recordings were then made at room temperature while the slices were continuously perfused with extracellular solution.

For whole-cell recordings from Purkinje cells, electrodes (3-6 MΩ) were filled with a solution containing (in mM): 140 CsCl, 4 NaCl, 0.5 $CaCl_2$, 10 HEPES, 5 EGTA, 2 MgATP, 0.4 Na_3GTP (pH 7.3). IPSCs were recorded under voltage clamp with a holding potential of -80 mV, unless otherwise indicated. Under these conditions, IPSCs were inward and the reversal potential for IPSCs was 1.8 mV (± 1.9 mV; n = 3), which is very similar to the value of -1.4 m V calculated for the chloride equilibrium potential. For cell-attached or whole-cell recordings from interneurons, electrodes (7-10 MΩ) were filled with a solution containing (in mM): 120 K-Gluconate, 9 KCl, 10 KOH, 3.48 $MgCl_2$, 4 NaCl, 10 HEPES, 4 Na_2ATP, 0.4 Na_3GTP, 17.5 Sucrose, 0.5 EGTA (pH 7.3). Alexa 594 (50 μM) or Lucifer yellow (2 mg/ml) was added in the internal solution to visualize cell morphology. Electrical responses were acquired via a Multiclamp 700B amplifier (Molecular Devices) with Digidata 1440A interface (Molecular Devices). Data were acquired at 10 μs intervals and filtered at 10 kHz (Bessel).

Mefloquine (MFQ; 50 μM; Sigma, St. Louis, MO), carbenoxolone (CBX; 200 μM; Sigma) and meclofenamic acid (MFA; 200 μM; Sigma) were used to block gap junctions. In some experiments, bicuculline (10 μM; Sigma), picrotoxin (PTX; 100 μM; Sigma), CNQX (10 μM; Ascent Scientific, Bristol, UK) and/or D-2-amino-5-phosphonopentanoate (D-APV; 50 μM;

Ascent Scientific) were used to block chemical transmission. Tetrodotoxin (1 µM; Tocris, Bristol, UK) was added to the external solution when examining spontaneous synaptic transmission.

Photostimulation

Photostimulation was accomplished as previously described (Wang et al., 2007). In brief, for wide-field excitation, slices were exposed to blue light (465-495 nm) from a mercury arc lamp, with light pulse duration controlled by an electronic shutter (Uniblitz T132; Vincent, Rochester, NY). For high-speed circuit mapping, photostimulation was done with a laser-scanning microscope (FV1000MPE; Olympus, Tokyo, Japan) equipped with × 25 NA 1.05 (Olympus XLPlan N) water-immersion objectives lens. A 510 x 510 µm area of the slice was scanned with a 405-nm laser spot (4 ms duration) in a 32 x 32 array of pixels, yielding a scanning resolution of 16 µm. The laser spot was scanned in a pseudorandom sequence, to avoid photostimulation of adjacent pixels, while cellular responses were simultaneously measured in cell-attached or whole-cell patch clamp recordings. The same microscope was used for 2-photon imaging of neuronal structure, using a Ti:sapphire laser (Mai Tai HP, Spectra Physics, 790 nm) as a light source.

Data analysis

Mapping data were analyzed with custom software written in MATLAB by P. Namburi. Spatial maps of the light sensitivity of ChR2-expressing interneurons were created by correlating the location of the photostimulation spot with voltage changes measured between 0 and 14 ms after the start of the light pulse (4 ms duration). Due to the relatively high spontaneous activity of interneurons, typically 3 or 4 maps were averaged to reduce the influence of this background activity: locations where action potentials were consistently evoked were considered light-sensitive areas and were included in measurements of optical footprint areas.

For creating maps of synaptic input, the location of the light spot was correlated with the resulting IPSCs in Purkinje cells. The threshold for detecting IPSCs was at least 3 σ of the background noise. Peak value and peak latency of the IPSC were determined from the maximum IPSC measured between 4 and 24 ms after the start of the photostimulus. Onset times were estimated as the zero-crossing time of a line joining values measured from 20% to 80% of the IPSC peak (Bartos et al., 2001). The area of the input field was measured by summing all pixels showing suprathreshold responses.

To calculate average probability maps, the spatial map measured in a given experiment was reoriented to place the cell soma in the center and Purkinje cell layer on the X-axis. Binary spatial maps of postsynaptic response (IPSC or no IPSC) were then averaged and displayed after being smoothed using a Gaussian filter (5 µm FWHM). Plots of the width of these spatial distributions were created at the location within the molecular layer where IPSC probability was maximum and above the Purkinje cell soma. Unless otherwise indicated, data are expressed as mean ± SEM.

Supplemental References

Bartos, M., Vida, I., Frotscher, M., Geiger, J.R., and Jonas, P. (2001). Rapid signaling at inhibitory synapses in a dentate gyrus interneuron network. J. Neurosci. *21*, 2687-2698.

Lee, S., Yoon, B.E., Berglund, K., Oh, S.J., Park, H., Shin, H.S., Augustine, G.J., Lee, C.J. (2010). Channel-mediated tonic GABA release from glia. Science *330*, 790-796.

Wang, H., Peca, J., Matsuzaki, M., Matsuzaki, K., Noguchi, J., Qiu, L., Wang, D., Zhang, F., Boyden, E., Deisseroth, K.*, et al.* (2007). High-speed mapping of synaptic connectivity using photostimulation in Channelrhodopsin-2 transgenic mice. Proc. Natl. Acad. Sci. USA *104*, 8143-8148.